Performance Comparison of Six Massive MIMO Channel Models

(Invited Paper)

Lu Bai[1], Cheng-Xiang Wang[2], Shangbin Wu[3], Carlos F. Lopez[2], Xiqi Gao[4], Wensheng Zhang[1] and Yu Liu[1]
[1]Shandong Provincial Key Lab. of Wireless Communications, Shandong University, Shandong, 250100, China.
[2]Institute of Sensors, Signals and Systems, School of Engineering and Physical Sciences, Heriot-Watt University, Edinburgh, EH14 4AS, UK.
[3]Samsung R&D Institute UK, Staines-upon-Thames, TW18 4QE, UK.
[4]School of Information Science and Engineering, Southeast University, Nanjing, 210096, China.
Email: bailusdu@126.com, cheng-xiang.wang@hw.ac.uk, shangbin.wu@samsung.com, c.f.lopez@hw.ac.uk, xqgao@seu.edu.cn, zhangwsh@sdu.edu.cn, xinwenliuyu@163.com

***Abstract*—In this paper, six recently proposed massive multiple-input multiple-output (MIMO) channel models are described briefly, and their normalized channel capacities and spatial cross-correlation functions (CCFs) are further compared. Among these models, two dimensional (2D) elliptical model, 2D parabolic model, three dimensional (3D) twin-cluster model, 3D 5G channel model, and 3D ellipsoid model are geometry-based stochastic models (GBSMs), while 2D Kronecker-based stochastic model with birth-death (BD) process on the array axis (KBSM-BD-AA) is a correlation-based stochastic model (CBSM). The 3D channel characteristics considering the elevation angles of massive MIMO channels, and 2D channel characteristics are investigated. The simulation results show that the spatial CCFs and channel capacities of 3D channel models are larger than those of the corresponding 2D channel models.**

***Keywords* – Massive MIMO channel models, GBSM, CBSM, spatial CCFs, normalized channel capacities.**

I. Introduction

Massive MIMO technology has widely been accepted as one of the most significant technologies of the fifth generation (5G) wireless communication networks due to its largely increasing spectral and energy efficiency [1]–[3]. Traditional MIMO channel models [4]–[6] cannot capture massive MIMO channel characteristics which have been investigated by a large number of measurements [7]–[10], such as cluster non-stationarity on both time and array axes, and spherical wavefront. It is important and necessary to propose a general, precise, and easy-to-use channel model to estimate the property of massive MIMO wireless communication systems.

Up to now, there are six channel models proposed for massive MIMO technology– the 2D elliptical model [12], the 3D twin-cluster model [13], the 3D 5G channel model [14], the 3D ellipsoid model [15], the 2D parabolic model [16], and the 2D KBSM-BD-AA [17]. The elliptical model is a 2D wideband GBSM, in which clusters are located on multi-confocal ellipses. The 3D twin-cluster model models the complicated scattering environment as the first and last bounces of twin-clusters and virtual links between them. Both the 2D elliptical model and 3D twin-cluster model can capture massive MIMO channel characteristics, such as spherical wavefront and non-stationarity on both array and time axes. They modeled cluster appearance and disappearance by a BD process. The proposed 3D general 5G channel model [14] can support channel characteristics of 5G wireless communication technologies, such as vehicle-to-vehicle (V2V) communications, massive MIMO technology, and millimeter wave (mmWave) technology. The 3D wideband multi-confocal ellipsoid channel model with uniform planar antenna arrays (UPAs) for massive MIMO wireless communication systems considered the non-stationary channel characteristics in the time and array domains by adopting a BD process and a seed algorithm on UPA for the first time. Only clusters in cluster evolution areas (CEAs) go through cluster evolution which is caused by near-field effect and other clusters can be observed by all antennas in UPA. In the 2D parabolic model, parabolic wavefronts replaced spherical wavefronts by a second-order approximation, which resulted in linear angle drifts of multipath components (MPCs). The authors modeled smooth average power variations by a spatial lognormal process and the non-stationarity on the array domain by a two-state Markov process. All the above models are GBSMs which are relatively accurate but complex. With lower complexity, a KBSM-BD-AA was proposed [17].

The remainder of this paper is organized as follows. Section II describes the six massive MIMO channel models. Results and analysis are shown in Section III. Finally, conclusions are given in Section IV.

II. Massive MIMO Channel Models

A. 2D Elliptical Model

Let M_{T} (M_{R}) denote the number of antennas in the uniform linear array (ULA) of the transmitter (Tx)/ receiver (Rx) which is located on focal point of the confocal ellipses whose major axis is $2f$. The antenna elements at Tx and Rx are spaced with separation δ_{T} and δ_{R}, respectively. The n-th cluster of scatterers is located on the n-th ellipse with major axis $2a_n$. The carrier wavelength and maximum Doppler frequency are presented as λ and $f_{\max}$, respectively.

978-1-5386-4502-4/17/$31.00 ©2017 IEEE

The non-stationarity on the array domain is modeled by a BD process. Let C_l^{T} denote the cluster set in which clusters are valid to the l-th antenna of the transmit array ($\mathrm{A}_l^{\mathrm{T}}$) and C_k^{R} denote the cluster set in which clusters are valid to the k-th antenna of the receive array ($\mathrm{A}_k^{\mathrm{R}}$). The survival probability of clusters in the cluster set at the Tx (Rx) $P_{\mathrm{survival}}^{\mathrm{T}}$ ($P_{\mathrm{survival}}^{\mathrm{R}}$) from C_{l-1}^{T} (C_l^{T}) to C_{k-1}^{T} (C_k^{R}) can be modeled as [18]

$$P_{\mathrm{survival}}^{\mathrm{T}} = \mathrm{e}^{-\boldsymbol{\lambda}_{\mathrm{R}} \frac{\boldsymbol{\delta}_{\mathrm{T}}}{\mathrm{D}_c^a}} \tag{1}$$

$$P_{\mathrm{survival}}^{\mathrm{R}} = \mathrm{e}^{-\boldsymbol{\lambda}_{\mathrm{R}} \frac{\boldsymbol{\delta}_{\mathrm{R}}}{\mathrm{D}_c^a}} \tag{2}$$

where D_c^a denotes the scenario-dependent correlation factor. $\boldsymbol{\lambda}_{\mathrm{R}}$ (per meter) and $\boldsymbol{\lambda}_{\mathrm{G}}$ (per meter) present the recombination rate and cluster generation rate.

The durations between two cluster appearances and disappearances both follow the exponential distribution [18], the average numbers of newly generated clusters $N_{\mathrm{new}}^{\mathrm{T}}$ and $N_{\mathrm{new}}^{\mathrm{R}}$ follow the Poisson process, which can be calculated as [18]

$$\mathrm{E}[N_{\mathrm{new}}^{\mathrm{T}}] = \frac{\boldsymbol{\lambda}_{\mathrm{G}}}{\boldsymbol{\lambda}_{\mathrm{R}}}(1 - \mathrm{e}^{-\frac{\boldsymbol{\delta}_{\mathrm{T}}}{\mathrm{D}_c^a}}) \tag{3}$$

$$\mathrm{E}[N_{\mathrm{new}}^{\mathrm{R}}] = \frac{\boldsymbol{\lambda}_{\mathrm{G}}}{\boldsymbol{\lambda}_{\mathrm{R}}}(1 - \mathrm{e}^{-\frac{\boldsymbol{\delta}_{\mathrm{R}}}{\mathrm{D}_c^a}}) \tag{4}$$

where $\mathrm{E}[\cdot]$ is the expectation.

According to the BD process, C_l^{T} (C_k^{R}) are obtained by $P_{\mathrm{survival}}^{\mathrm{T}}$ ($P_{\mathrm{survival}}^{\mathrm{R}}$) and $N_{\mathrm{new}}^{\mathrm{T}}$ ($N_{\mathrm{new}}^{\mathrm{R}}$). The total number of clusters N_{total} are the sum of the clusters which are valid to at least one pair of antennas, which can be expressed as

$$N_{\mathrm{total}} = \mathrm{card}(\bigcup_{l=1}^{M_T}\bigcup_{k=1}^{M_R}(C_l^{\mathrm{T}}(t) \cap C_k^{\mathrm{R}}(t))) \tag{5}$$

where $\mathrm{card}(\cdot)$ is the cardinality of a set. Then, a cluster, say $\mathrm{Cluster}_n$ ($n \leq N_{\mathrm{total}}$), is valid to both $\mathrm{A}_l^{\mathrm{T}}$ and $\mathrm{A}_k^{\mathrm{R}}$ if and only if $\mathrm{Cluster}_n \in C_l^{\mathrm{T}} \cap C_k^{\mathrm{R}}$. The total channel impulse response (CIR) consists of two elements, i.e., line-of-sight (LOS) CIR and non-LOS (NLOS) CIR. It can be expressed as a complex matrix $\mathbf{H} = [h_{kl}(\boldsymbol{t}, \boldsymbol{\tau})]_{M_{\mathrm{R}} \times M_{\mathrm{T}}}$, where $k = 1, 2, \cdots, M_{\mathrm{R}}$ and $l = 1, 2, \cdots, M_{\mathrm{T}}$. In the theoretical model, the number of rays which are in one cluster (S) **is infinite, and the multipath** complex gains $h_{kl}(\boldsymbol{t}, \boldsymbol{\tau})$ between $\mathrm{A}_l^{\mathrm{T}}$ and $\mathrm{A}_k^{\mathrm{R}}$ at delay $\boldsymbol{\tau}$ can be expressed as

$$h_{kl}(\boldsymbol{t}, \boldsymbol{\tau}) = \sum_{n=1}^{N_{\mathrm{total}}} h_{kl,n}(t)\boldsymbol{\delta}(\boldsymbol{\tau} - \boldsymbol{\tau}_n) \tag{6}$$

– if $\mathrm{Cluster}_n \in (C_l^{\mathrm{T}}(t) \cap C_k^{\mathrm{R}}(t))$

$$h_{kl,n}(t) = \underbrace{\boldsymbol{\delta}(n-1)\sqrt{\frac{K}{K+1}}\mathrm{e}^{j\left(2\boldsymbol{\pi}\boldsymbol{f}_{kl}^{\mathrm{LOS}}(t)t + \boldsymbol{\phi}_{kl}^{\mathrm{LOS}}(t)\right)}}_{\mathrm{LOS}} + \underbrace{\sqrt{\frac{P_n}{K+1}} \lim_{S\to\infty}\left(\frac{1}{\sqrt{S}}\sum_{i=1}^{S}\mathrm{e}^{j\left(2\boldsymbol{\pi}f_{n,i}(t)t + \boldsymbol{\phi}_{kl,n,i}(t)\right)}\right)}_{\mathrm{NLOS}} \tag{7}$$

– if $\mathrm{Cluster}_n \notin (C_l^{\mathrm{T}}(t) \cap C_k^{\mathrm{R}}(t))$

$$h_{kl,n}(t) = 0. \tag{8}$$

where K is LOS Rician factor and P_n is normalized mean power of the n-th cluster. More details of calculations of this 2D elliptical model are in [12].

B. 3D Twin-Cluster Model

For the twin-cluster model, the propagation environment between Tx and Rx through each cluster, for example $\mathrm{Cluster}_n$ ($n \leq N_{\mathrm{total}}$)**, is composed of three parts, i.e. the first bounce** between Tx and a representation $\mathrm{Cluster}_n^{\mathrm{T}}$, the last bounce between Rx and a representation $\mathrm{Cluster}_n^{\mathrm{R}}$, and the virtual link between the two representations. There are S_1 rays in the **first bounce, and** S_2 rays in the last bounce.

The CIR of this model is similar with elliptical model but the calculations of the parameters are based on the 3D vector coordinate system. At the meanwhile, the NLOS components of CIR should be calculated as

$$h_{kl,n}^{\mathrm{NLOS}}(t) = \sqrt{\frac{P_n}{K+1}} \lim_{S_1,S_2\to\infty}\left(\sum_{i_1=1}^{S_1}\sum_{i_2=1}^{S_2}\frac{\mathrm{e}^{j\left(2\boldsymbol{\pi}f_{n,i_1}(t)t + \boldsymbol{\phi}_{kl,n,i_1i_2}(t)\right)}}{\sqrt{S_1S_2}}\right). \tag{9}$$

More details of calculations of this 3D twin-cluster model are in [13].

C. 3D 5G Channel Model

The 5G GBSM is a 3D channel model, which is based on the twin-cluster model and Saleh-Valenzuela channel model [19], which was originally proposed for indoor multipath propagations to support the high time resolution which is an important characteristic of mmWave channels. The number of rays within each cluster follows a Poisson distribution. Delay and complex gain are assigned to each ray. Doppler frequencies are taken into account at both the Tx and Rx for supporting V2V features. Moreover, polarized directional antennas are considered. The CIR can be computed as

$$h_{kl}(\boldsymbol{t}, \boldsymbol{\tau}) = \underbrace{\sqrt{\frac{K(t)}{K(t)+1}}h_{kl}^{\mathrm{LOS}}(t)\boldsymbol{\delta}(\boldsymbol{\tau} - \boldsymbol{\tau}^{\mathrm{LOS}})}_{\mathrm{LOS}} + \underbrace{\sqrt{\frac{1}{K(t)+1}}\sum_{n=1}^{N_{\mathrm{total}}(t)}\sum_{m_n=1}^{M_n(t)}h_{kl,n,m_n}(t)\boldsymbol{\delta}(\boldsymbol{\tau} - \boldsymbol{\tau}_n(t) - \boldsymbol{\tau}_{m_n}(t))}_{\mathrm{NLOS}} \tag{10}$$

where $N_{\mathrm{total}}(t)$ is the number of clusters, $M_n(t)$ is the number of rays which are in $\mathrm{Cluster}_n$ which follows a Poisson distribution, $\boldsymbol{\tau}_n(t)$ is the delay of $\mathrm{Cluster}_n$, and $\boldsymbol{\tau}_{m_n}(t)$ is the delay of the m_n-th ray in $\mathrm{Cluster}_n$. All the parameters of the proposed 5G channel model vary as time, which can model the non-stationary on time axis and high mobility of channels.

For the LOS CIR, if both the Tx and Rx take polarized antenna arrays into account, the channel gain $h_{kl}^{\mathrm{LOS}}(t)$ can be

expressed as

$$h_{kl}^{\mathrm{LOS}}(t) = \begin{bmatrix} F_{l,\mathrm{V}}^{\mathrm{T}}(\mathbf{D}_{kl}^{\mathrm{LOS}}(t), \mathbf{A}_l^{\mathrm{T}}(t)) \\ F_{l,\mathrm{H}}^{\mathrm{T}}(\mathbf{D}_{kl}^{\mathrm{LOS}}(t), \mathbf{A}_l^{\mathrm{T}}(t)) \end{bmatrix}^{\mathrm{T}} \begin{bmatrix} \mathrm{e}^{j\boldsymbol{\phi}_{\mathrm{LOS}}} & 0 \\ 0 & -\mathrm{e}^{j\boldsymbol{\phi}_{\mathrm{LOS}}} \end{bmatrix} \begin{bmatrix} F_{k,\mathrm{V}}^{\mathrm{R}}(\mathbf{D}_{kl}^{\mathrm{LOS}}(t), \mathbf{A}_k^{\mathrm{R}}(t)) \\ F_{k,\mathrm{H}}^{\mathrm{R}}(\mathbf{D}_{kl}^{\mathrm{LOS}}(t), \mathbf{A}_k^{\mathrm{R}}(t)) \end{bmatrix} \mathrm{e}^{j\left(2\pi \boldsymbol{f}_{kl}^{\mathrm{LOS}}(t)t\right)} \tag{11}$$

where $\boldsymbol{\phi}_{\mathrm{LOS}}$ is uniformly distributed over the internal $[0, 2\pi)$ [20]. The superscript $V(H)$ denotes vertical polarization (horizontal polarization). Functions $F^{\mathrm{T}}(a, b)$ and $F^{\mathrm{R}}(a, b)$ are antenna patterns with input vectors a and b in the global coordinate system. The input vectors a and b are transformed into the local coordinate system to obtain the antenna patterns.

For NLOS components, if $\mathrm{Cluster}_n \notin C_l^{\mathrm{T}}(t) \cap C_k^{\mathrm{R}}(t)$, the complex channel gain $h_{kl,n,m_n}(t)$ can be presented as

$$h_{kl,n,m_n}(t) = \begin{bmatrix} F_{l,\mathrm{V}}^{\mathrm{T}}(\mathbf{D}_{n,m_n}^{\mathrm{T}}(t), \mathbf{A}_l^{\mathrm{T}}(t)) \\ F_{l,\mathrm{H}}^{\mathrm{T}}(\mathbf{D}_{n,m_n}^{\mathrm{T}}(t), \mathbf{A}_l^{\mathrm{T}}(t)) \end{bmatrix}^{\mathrm{T}} \begin{bmatrix} \mathrm{e}^{j\boldsymbol{\phi}_{n,m_n}^{\mathrm{VV}}} & \sqrt{\boldsymbol{\kappa}}\mathrm{e}^{j\boldsymbol{\phi}_{n,m_n}^{\mathrm{VH}}} \\ \sqrt{\boldsymbol{\kappa}}\mathrm{e}^{j\boldsymbol{\phi}_{n,m_n}^{\mathrm{HV}}} & \mathrm{e}^{j\boldsymbol{\phi}_{n,m_n}^{\mathrm{HH}}} \end{bmatrix} \begin{bmatrix} F_{k,\mathrm{V}}^{\mathrm{R}}(\mathbf{D}_{n,m_n}^{\mathrm{R}}(t), \mathbf{A}_k^{\mathrm{R}}(t)) \\ F_{k,\mathrm{H}}^{\mathrm{R}}(\mathbf{D}_{n,m_n}^{\mathrm{R}}(t), \mathbf{A}_k^{\mathrm{R}}(t)) \end{bmatrix} \sqrt{P_{n,m_n}(t)}\mathrm{e}^{j\left(2\pi \boldsymbol{f}_{kn,m_n}^{\mathrm{R}}(t)t\right)}\mathrm{e}^{j\left(2\pi \boldsymbol{f}_{ln,m_n}^{\mathrm{T}}(t)t\right)} \tag{12}$$

where P_{n,m_n} is normalized mean power of the m_n-th ray in $\mathrm{Cluster}_n$ and $\sqrt{\boldsymbol{\kappa}}$ is the cross polarization power ratio. The normalized mean power of $\mathrm{Cluster}_n$ can be computed as $P_n = \sum_{m_n} P_{n,m_n}$. Random phases $\boldsymbol{\phi}_{n,m_n}^{\mathrm{VV}}, \boldsymbol{\phi}_{n,m_n}^{\mathrm{VH}}, \boldsymbol{\phi}_{n,m_n}^{\mathrm{HV}}, \boldsymbol{\phi}_{n,m_n}^{\mathrm{HH}}$ are uniformly distributed within $[0, 2\pi)$ [6].

The 5G channel model can easily be adapted to various **configurations for different scenarios with various technologies** by setting proper channel parameters.

D. 2D Parabolic Model

The parabolic model is a 2D wideband non-stationary GBSM based on WINNER model [6]. There are two contributions in this model. On one hand, parabolic wavefronts are modeled by a second-order approximation. This approximation results in approximately linear angle drifts of MPC, reducing computational and theoretical complexity compared to spherical wavefronts [21]. On the other hand, smooth cluster power variations can be calculated by a spatial lognormal process and cluster evolution is modeled by a two-state Markov process. The CIR can be calculated as

$$h_{kl}(\boldsymbol{t}, \boldsymbol{\tau}) = h_{kl}^{\mathrm{LOS}}(t) + \sum_{n=1}^{N_{\mathrm{total}}} h_{kl,n}(t)\boldsymbol{\delta}(\boldsymbol{\tau} - \boldsymbol{\tau}_n) \tag{13}$$

where

$$h_{kl}^{\mathrm{LOS}}(t) = \sqrt{P_l^{\mathrm{LOS}}}\mathrm{e}^{j\left(\boldsymbol{\Delta\phi}_{lk}^{\mathrm{LOS}} + 2\pi \boldsymbol{f}_l^{\mathrm{LOS}}t\right)} \tag{14}$$

$$h_{kl,n}(t) = \sqrt{\frac{P_{l,n}}{M_n}} \sum_{m_n=1}^{M_n} \mathrm{e}^{j\boldsymbol{\theta}_{m_n}}\mathrm{e}^{j\left(\boldsymbol{\Delta\phi}_{lk,m_n} + 2\pi \boldsymbol{f}_{l,m_n}t\right)} \tag{15}$$

where M_n is the number of rays per cluster and $\boldsymbol{\theta}_{m_n}$ indicates i.i.d. random variable which follows uniformly distribution over $[0, 2\pi)$. **It definates the phase of the** m-th MPC which are in the n-th cluster at the center of the Tx antenna array . $\boldsymbol{\Delta\phi}_{lk}^{\mathrm{LOS}}$ and $\boldsymbol{\Delta\phi}_{lk,m_n}$ present the phase variations experienced by the LOS CIR and the m-th MPC within the n-th cluster from the l-th Tx antenna to the k-th receiver antenna, respectively. P_l^{LOS} and $P_{l,n}$ are the powers of the LOS component and the average cluster power at the l-th Tx antenna, respectively. f_{l,m_n} is the Doppler frequency shift of the m-th MPC for the n-th cluster. The detailed calculations of parameters of the parabolic model can be found in [16].

E. 2D KBSM-BD-AA

In the conventional KBSM for MIMO wireless communication system, the spatial correlation between the Tx array and Rx array is not considered. The CIR can be expressed as

$$\mathbf{H} = \mathbf{R}_{\mathrm{R}}^{\frac{1}{2}}\mathbf{H}_{\mathrm{w}}\mathbf{R}_{\mathrm{T}}^{\frac{T}{2}} \tag{16}$$

where $\mathbf{H}_{\mathrm{w}}$ denotes a $M_{\mathrm{R}} \times M_{\mathrm{T}}$ matrix with zero-mean unit-variance complex i.i.d Gaussian entries, $\mathbf{R}_{\mathrm{R}}(\mathbf{R}_{\mathrm{T}})$ is Toeplitz matrices which denotes overall spatial correlation matrices at the Rx (Tx) when the Rx (Tx) array is ULA [22]. The element of spatial correlation between the m-th and the n-th antennas in $\mathbf{R}_{\mathrm{R}}$, i.e. $R_{\mathrm{R},mn}$ can be calculated as

$$R_{\mathrm{R},mn} = T_{\mathrm{R},mn} = \frac{\sum\limits_k s_{mk}^{\mathrm{R}}\left(s_{nk}^{\mathrm{R}}\right)^*}{\sqrt{\sum\limits_k |s_{mk}^{\mathrm{R}}|^2}\sqrt{\sum\limits_k |s_{nk}^{\mathrm{R}}|^2}} \tag{17}$$

where s_{mk}^{R} is the complex gain between the m-th ($m = 1, 2, \cdots, M_R$) antenna and the k-th ($k = 1, 2, \cdots$) scatterer , and s_{nk}^{R} is the complex gain between the n-th ($n = 1, 2, \cdots, M_R$) antenna and the k-th scatterer. $T_{\mathrm{R},mn}$ is the **spatial correlation coefficient between the** m-th and the n-th antennas and the entry of matrix $\mathbf{T}_{\mathrm{R}}$ in the m-th row and n-th column.

For the massive MIMO channel, antennas are not effected by the same set of scatterers. So, $\mathbf{R}_{\mathrm{R}} = \mathbf{T}_{\mathrm{R}}$ is not valid any more. The survival probability $E_{\mathrm{R},mn}$ of scatterers when they evolve from the m-th antenna to the n-th antenna can be modeled by a BD process [17],

$$E_{\mathrm{R},mn} = e^{-\boldsymbol{\beta}|m-n|} \tag{18}$$

where $\boldsymbol{\beta} \geqslant 0$ presents how fast scatterers disappear on the array axis. $E_{\mathrm{R},mn}$ is decreasing if the difference between m and n is increasing, which means that less scatterers are shared if the antenna spacing is bigger. Then,

$$R_{\mathrm{R},mn} = E_{\mathrm{R},mn}T_{\mathrm{R},mn} = E_{\mathrm{R},mn}\frac{\sum\limits_k s_{mk}^{\mathrm{R}}\left(s_{nk}^{\mathrm{R}}\right)^*}{\sqrt{\sum\limits_k |s_{mk}^{\mathrm{R}}|^2}\sqrt{\sum\limits_k |s_{nk}^{\mathrm{R}}|^2}}. \tag{19}$$

The calculation for Tx is same with the above procedure.

F. 3D Ellipsoid Model

In the proposed 3D ellipsoid model, each ellipsoid was the rotation of an ellipse with respect to the y axis. The Tx and Rx are equipped with UPAs with M_{T} $(m \times n)$ and M_{R} $(p \times q)$ omnidirectional antennas, respectively. The central points of UPAs are located at the focal points of the confocal ellipsoids with major axis $2f$. The o-th cluster of scatterers is located on the o-th ellipsoid with major axis $2a_o$. The antenna spacings of the Tx and Rx are denoted as $\boldsymbol{\delta}_{\mathrm{T}}$ and $\boldsymbol{\delta}_{\mathrm{R}}$, respectively. The massive MIMO CIR can be presented as a $M_{\mathrm{R}} \times M_{\mathrm{T}}$ $[(p \times q) \times (m \times n)]$ complex matrix. Each item of $\mathbf{H}(t,\tau)$ can be presented as

$$h_{lk,uw}(\boldsymbol{t},\boldsymbol{\tau}) = \sum_{o=1}^{N_{\mathrm{total}}} h_{lk,ij,o}(t)\boldsymbol{\delta}(\tau - \tau_o(t)) \tag{20}$$

– if $\mathrm{Cluster}_o \in (C_{uw}^{\mathrm{T}} \cap C_{lk}^{\mathrm{R}})$

$$h_{lk,uw,o}(t) = \underbrace{\boldsymbol{\delta}(o-1)\sqrt{\frac{K}{K+1}}\mathrm{e}^{j\left(2\boldsymbol{\pi}\boldsymbol{f}_{lk,uw}^{\mathrm{LOS}}(t)t+\boldsymbol{\phi}_{lk,uw}^{\mathrm{LOS}}(t)\right)}}_{\mathrm{LOS}}$$
$$+\underbrace{\sqrt{\frac{P_o}{K+1}}\lim_{S\to\infty}\left(\frac{1}{\sqrt{S}}\sum_{s=1}^{S}\mathrm{e}^{j\left(2\boldsymbol{\pi}f_{o,s}(t)t+\boldsymbol{\phi}_{lk,uw,o,s}(t)\right)}\right)}_{\mathrm{NLOS}} \tag{21}$$

– if $\mathrm{Cluster}_o \notin (C_{uw}^{\mathrm{T}} \cap C_{lk}^{\mathrm{R}})$

$$h_{lk,uw,o}(t) = 0. \tag{22}$$

The elliptical model [12], the twin-cluster model [13], the 5G channel model [14], the parabolic model [16], and the KBSM-BD-AA [17] always considered non-stationary channel characteristics on the array axis, no matter what the relationship between the distance between Tx and Rx and Rayleigh **distance. In fact, near-field effects are valid only in the area whose radius is Rayleigh distance [23]. So, this paper first** introduces the threshold of the cluster evolution as Γ, which **defines the radius of CEAs. Note that**

$$\Gamma_{\mathrm{T}} = \frac{2\delta_{\mathrm{T}}^2\left(m^2+n^2\right)}{\boldsymbol{\lambda}} \tag{23}$$

$$\Gamma_{\mathrm{R}} = \frac{2\delta_{\mathrm{R}}^2\left(p^2+q^2\right)}{\boldsymbol{\lambda}}. \tag{24}$$

The areas whose radius are Γ_{T} and Γ_{R} are the CEAs where clusters can be only affected by part of the antennas. The more calculation and the seed algorithm for UPAs can be found in [15].

The characteristics of above six models including wavefront, cluster evolution, supporting 3D, moving Rx, mmW, UPAs or not are compared as shown in Table I.

III. Resluts and Analysis

The absolute values of spatial CCFs of the 3D ellipsoid model, the 2D 5G channel model, the 3D twin-cluster model, the 2D parabolic model, the 2D elliptical model, and the 2D KBSM-BD-AA in isotropic scattering environments at the Rx

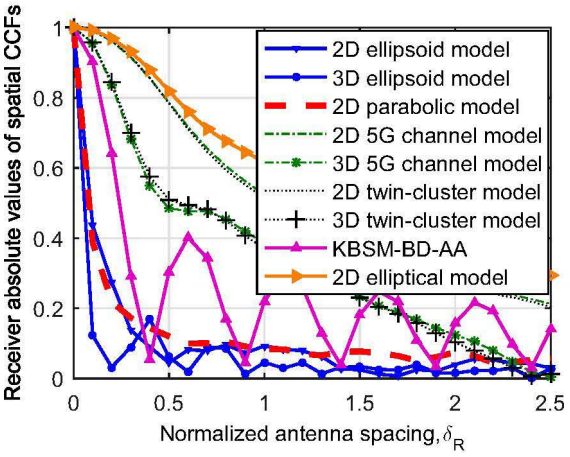

Fig. 1: Receiver spatial CCFS of six massive MIMO channel models ($M_{\mathrm{T}} = 128, M_{\mathrm{R}} = 8, f_c = 2GHz, D = 160$ m, $\mathbf{v} = 5$ m/s, $\mathbf{v}_c$=0.5 m/s, T_0 (initial time)=0 s, $\boldsymbol{\mu}_A^{\mathrm{T}} = \boldsymbol{\pi}/3, \boldsymbol{\mu}_E^{\mathrm{T}} = \boldsymbol{\pi}/4$ (3D models only), $\boldsymbol{\mu}_A^{\mathrm{R}} = \boldsymbol{\pi}/4, \boldsymbol{\mu}_E^{\mathrm{R}} = \boldsymbol{\pi}/3$ (3D models only), $\boldsymbol{\nu}_A^{\mathrm{T}} = 0, \boldsymbol{\nu}_E^{\mathrm{T}} = 0$ (3D models only), $\boldsymbol{\nu}_A^{\mathrm{R}} = \boldsymbol{\pi}/3, \boldsymbol{\nu}_E^{\mathrm{R}} = 0$ (3D models only).

are completed in Fig. 1. For the three 3D models, we also present their corresponding 2D models with elevation angle being zero. The spatial CCF of the 2D ellipsoid model is slightly larger than that of the 3D ellipsoid model when the **channel environment and array configuration are the same.** This conclusion also holds for the 2D/3D twin-cluster model and the 2D/3D 5G channel model. The characteristics of elevation angles in 3D channel models can increase the diversity **of channel models and therefore, have negative influence on** the spatial CCFs.

The spatial CCF of the 3D general 5G channel model is very similar with that of the 3D twin-cluster model. A similar conclusion can be obtained in 2D cases. The reason is that **the simplified massive MIMO channel model resulting from** the 5G channel model is based on the twin-cluster model. Their difference is only on describing the delays of sub-paths in certain clusters. The spatial CCF of the KBSM-BD-AA is an exponentially decaying function multiplied with a zero-th **order Bessel function of the first kind.**

Fig. 2 shows the comparison of normalized channel capacities of the above six massive MIMO channel models and an i.i.d. massive MIMO modes in isotropic scattering environments. The channel capacities of 3D models are in general large compared to those of 2D models. From this **figure, we can conclude that the elevation angles have some influence on the capacity of channels. The channel capacity** of the i.i.d. channel model is the upper bound of channel capacities. The reason why the channel capacity of KBSM-BD-AA is larger than those all of the GBSMs is that the way introducing cluster evolution in the KBSM-BD-AA is simpler than those in GBSMs. Channel capacities of all the above models are not comparable when SNR is less than 12 dB.

TABLE I: Comparison of six massive MIMO channel models.

Characteristics \ Model	[12]	[13]	[14]	[15]	[16]	[17]
Support 3D	N	Y	Y	Y	N	N
Support moving Rx	Y	Y	Y	Y	Y	N
Support mmW	N	N	Y	N	N	N
Support UPAs	N	N	N	Y	N	N
Model cluster (dis)appearance	BD process	BD process	BD process	BD process	Two-state Markov process	BD process
Wavefront	Spherical	Spherical	Spherical	Spherical	Parabolic	Plane

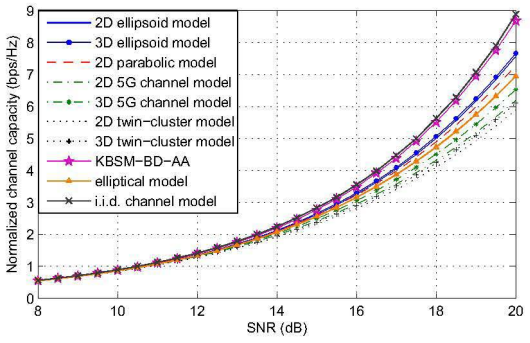

Fig. 2: Comparison of channel capacities of ellipsoid model, 5G channel model, twin-cluster model, the parabolic model, elliptical model, KBSM-BD-AA and the i.i.d. massive MIMO model ($M_{\mathrm{T}} = 32, M_{\mathrm{R}} = 32, f_c = 2GHz, D = 160$ m, $\mathbf{v} = 5$ m/s, $\mathbf{v}_c$=0.5 m/s, T_0(initial time)=0 s, $\boldsymbol{\mu}_A^{\mathrm{T}} = \boldsymbol{\pi}/3, \boldsymbol{\mu}_E^{\mathrm{T}} = \boldsymbol{\pi}/4$ (3D models only), $\boldsymbol{\mu}_A^{\mathrm{R}} = \boldsymbol{\pi}/4, \boldsymbol{\mu}_E^{\mathrm{R}} = \boldsymbol{\pi}/3$(3D models only),$\boldsymbol{\nu}_A^{\mathrm{T}} = 0, \boldsymbol{\nu}_E^{\mathrm{T}} = 0$ (3D models only), $\boldsymbol{\nu}_A^{\mathrm{R}} = \boldsymbol{\pi}/3, \boldsymbol{\nu}_E^{\mathrm{R}} = 0$(3D models only).

IV. Conclusions

This paper has investigated and compared the spatial CCFs and capacities of six massive MIMO channel models. Simulation results have shown that the spatial CCFs and capacities of 3D GBSMs, such as ellipsoid model, 5G channel model, and twin-cluster model are larger than those of 2D ones. Furthermore, the capacities of the KBSM-BD-AA is larger than those of GBSMs.

V. Acknowledgement

The authors would like to acknowledge the support from the Natural Science Foundation of China (Grant No. 61371110), Fundamental Research Funds of Shandong University (No. 2017JC029), EU H2020 ITN 5G wireless project (Grant No. 641985), EU FP7 QUICK project (Grant No. PIRSES-GA-2013-612652) EU H2020 RISE TESTBED project (Grant No. 734325), and EPSRC TOUCAN project (Grant No. EP/L020009/1).

References

[1] E. G. Larsson, F. Tufvesson, and O. Edfors, "Massive MIMO for next generation wireless systems," *IEEE Commun. Mag.*, vol. 2, no. 52, pp. 186-195, 2014.

[2] F. Rusek, D. Persson, and B. K. Lau, "Scaling up MIMO: opportunities and challenges with very large arrays," *IEEE Sig. Proc. Mag.*, vol. 30, no. 1, pp. 40-60, 2012.

[3] C.-X. Wang,?S. Wu, L. Bai, X. You, J. Wang, and C.-L. I, "Recent advances and future challenges for massive MIMO channel measurements and models," *?Sci. China Inf. Sci.*, vol. 59, no. 2, pp. 1-16, Feb. 2016.

[4] 3GPP T.S. 25.996, *Spatial channel model for multiple-input multiple-output (MIMO) simulations*, V11.0.0, 2012.

[5] Report ITU-R M.2135-1, "Guidelines for evaluation of radio interface technologies for IMT-Advanced," 2009.

[6] WINNER D1.1.2 P. Kyosti, "WINNER II channel models," ver 1.1, Sept. 2007. Available: https://www.ist-winner.org/WINNER2-Deliverables/D1.1.2v1.1.pdf

[7] S. Payami and F. Tufvesson, "Channel measurements and analysis for very large array systems at 2.6GHz," in *Proc. EuCAP'12*, Prague, 2012, pp. 1-8.

[8] X. Gao, O. Edfors, F. Rusek, et al, "Linear pre-coding performance in measured very large MIMO channels," in *Proc. IEEE VTC'12-Fall.*, San Francisco, US, 2011, pp. 1-5.

[9] X. Gao, O. Edfors, F. Rusek, et al, "Massive MIMO in real propagation environments," *IEEE Trans. Wireless Commun.*, vol. 63, no. 11, pp. 3917-3928, Mar. 2015.

[10] J. Vieira, S. Malkowsky, K. Nieman, el al, "A flexible 100-antenna testbed for massive MIMO," in *Proc. IEEE Globecom'14*, Austin, USA, 2014.

[11] X. Gao, A. Glazunov, J. Weng, et al, "Channel measurement and characterization of interference between residential femto-cell systems," in *Proc. EuCAP'11*, Rome, Italy, 2011.

[12] S. Wu, C. -X. Wang, H. Haas, el-H. M. Aggoune, M. M. Alwakeel, and B. Ai, "A non-stationary wideband channel model for massive MIMO communication systems," *IEEE Trans. Wireless Commun.*, vol. 14, no. 3, pp. 1434-1446, Mar. 2015.

[13] S. Wu, C.-X. Wang, el-H. M. Aggoune, M. M. Alwakeel, and Y. He, "A non-stationary 3-D wideband twin-cluster model for 5G massive MIMO channels," *IEEE J. Sel. Areas Commun.*, vol. 32, no. 6, pp. 1207-1218, Jun. 2014.

[14] S. Wu, C.-X. Wang, el-H. M. Aggoune, M. M. Alwakeel, and X.-H. You, "A general 3D non-stationary 5G wireless channel model," *IEEE Trans. Commun.*, submitted for publication.

[15] L. Bai, C.-X. Wang, S. Wu, J. Sun, W. Zhang, "A 3-D wideband multi-confocal ellipsoid model for wireless massive MIMO communication channels with uniform planar antenna array," *in Proc. IEEE VTC'17-Spring*, Sydney, Australia, Jun. 2017.

[16] C. F. Lopez, C.-X. Wang, and R. Feng, "A novel 2D non-stationary wideband massive MIMO channel model," *in Proc. IEEE CAMAD'16*, Toronto, Canada, Oct. 2016.

[17] S. Wu, C.-X. Wang, el-H. Aggoune, and M. M. Alwakeel, "A novel Kronecker-based stochastic model for massive MIMO channels," *in Proc. IEEE/CIC ICCC'15*, Shenzhen, China, Nov. 2015, pp. 1-6.

[18] A. Papoulis and S. U. Pillai, *Probability, random variables, and stochastic processes.*, 4th ed, McGrawCHill, New York, 2002.

[19] A. A. M. Saleh and R. A. Valenzuela, "A statistical model for indoor multipath propagation," *IEEE J. Sel. Areas Commun.*, vol. 5, no. 2, pp. 128-137, Feb. 1987

[20] 3GPP T.R. 36.873, *Study on 3D channel model for LTE*, V12.2.0, June 2015.

[21] A. L. Swindlehurst and T. Kailath, "Passive direction-of-arrival and **range estimation for near-field sources," in** *Proc. IEEE ASSP'88*, Minneapolis, MN, USA, Aug. 1988, pp. 123-128.

[22] C.-N. Chuah, D. N. C. Tse, J. M. Kahn, and R. A. Valenzuela, "Capacity scaling in MIMO wireless systems under correlated fading," *IEEE Trans. Inf. Theory*, vol. 48, no. 3, pp. 637-650, Mar. 2002.

[23] A. Yaghjw, "An overview of near-field antenna measurements," *IEEE Trans. Antennas Propag.*, vol. AP-34, no. 1, Jan. 1986.